

Non-volatile Fermi level tuning for the control of spin-charge conversion at room temperature

Received: 30 October 2023

Accepted: 20 September 2024

Published online: 09 October 2024

 Check for updates

Jonghyeon Choi¹, Jungmin Park²✉, Seunghyeon Noh¹, Jaebyeong Lee¹,
Seunghyun Lee¹, Daeseong Choe^{1,3}, Hyeonjung Jung¹, Junhyeon Jo¹,
Inseon Oh^{1,4}, Juwon Han^{1,5}, Soon-Yong Kwon^{1,5}, Chang Won Ahn⁶,
Byoung-Chul Min³, Hosub Jin⁷, Choong H. Kim^{8,9,10}✉,
Kyoung-Whan Kim^{3,11}✉ & Jung-Woo Yoo^{1,5}✉

Current silicon-based CMOS devices face physical limitations in downscaling size and power loss, restricting their capability to meet the demands for data storage and information processing of emerging technologies. One possible alternative is to encode the information in a non-volatile magnetic state and manipulate this spin state electronically, as in spintronics. However, current spintronic devices rely on the current-driven control of magnetization, which involves Joule heating and power dissipation. This limitation has motivated intense research into the voltage-driven manipulation of spin signals to achieve energy-efficient device operation. Here, we show non-volatile control of spin-charge conversion at room temperature in graphene-based heterostructures through Fermi level tuning. We use a polymeric ferroelectric film to induce non-volatile charging in graphene. To demonstrate the switching of spin-to-charge conversion we perform ferromagnetic resonance and inverse Edelstein effect experiments. The sign change of output voltage is derived by the change of carrier type, which can be achieved solely by a voltage pulse. Our results provide an alternative approach for the electric-field control of spin-charge conversion, which constitutes a building block for the next generation of spin-orbitronic memory and logic devices.

Today's semiconductor industry faces ever-increasing demands for computing power and data storage due to emerging technology, such as artificial intelligence. The new platform for memory and/or logic device need to overcome challenges such as continuous downscaling,

Joule heating, and low-power consumption in traditional Si-based device. Manipulation of collective state variables could provide progressive miniaturization, superior energy efficiency, and non-volatility¹. Spin-based devices that exploit the collective state of

¹Department of Materials and Science and Engineering, Ulsan National Institute of Science and Technology, Ulsan, Republic of Korea. ²Department of Physics, Korea Advanced Institute of Science and Technology, Daejeon, Republic of Korea. ³Center for Semiconductor Technology, Korea Institute of Science and Technology, Seoul, Korea. ⁴The Molecular Foundry, Lawrence Berkeley National Laboratory, Berkeley, CA, USA. ⁵Graduate School of Semiconductor Materials and Devices Engineering, Ulsan National Institute of Science and Technology, Ulsan, Republic of Korea. ⁶Department of Physics and Energy Harvest-Storage Research Center, University of Ulsan, Ulsan, Republic of Korea. ⁷Department of Physics, Ulsan National Institute of Science and Technology, Ulsan, Republic of Korea. ⁸Center for Correlated Electron Systems, Institute for Basic Science (IBS), Seoul, Republic of Korea. ⁹Department of Physics and Astronomy, Seoul National University, Seoul, Korea. ¹⁰Korea Institute for Advanced Study, Seoul, Korea. ¹¹Department of Physics, Yonsei University, Seoul, Korea.

✉ e-mail: jungmin0123@kaist.ac.kr; chkim82@snu.ac.kr; kwkim@yonsei.ac.kr; jwwoo@unist.ac.kr

ferromagnetism carrying a non-volatile nature have shown great potential and versatile opportunities. In particular, the control of magnetization through spin-transfer torque (STT) and/or spin-orbit torque (SOT) have brought major advances in the integration of chip architecture with improved device endurance, switching speed and reliability, and fabrication compatibility^{2–6}. However, the reversal of magnetization via STT or SOT requires current flow over the threshold value, which involves significant energy dissipation. In order to alleviate such energy consumption, voltage-controlled magnetic anisotropy (VCMA) has been extensively explored as it reduces the barrier for magnetization reversal^{7,8}. Yet, this approach still requires an external magnetic field or current-driven torque to switch magnetic polarity. The complete control of magnetization solely by an electric field will bring significant merits in improving power loss as well as heating issues in device operations. Employing multi-ferroic materials to control the magnetization with only an electric field has recently been proposed with a prospect of beyond CMOS technology¹. It should be noted that the recent report of Vaz et al. showed the voltage control of magnetization using multi-ferroic materials and its electrical readout⁹.

Spin-orbit interaction could drive conversion between spin and charge flow as it couples spin and momentum of itinerant electrons. Thus, the generation of pure spin currents from the charge flow can be achieved without ferromagnets. Conversely, spin currents could be converted into electrical output without ferromagnets. In particular, Rashba-type spin-orbit interaction which occurs at the interfaces or surfaces due to broken inversion symmetry leads to intertwined spin texture at the Fermi surface^{10,11}. Here, the conversion between spin and charge flow could also occur through the shift of spin-textured Fermi surface^{12–14}. And such conversion could be magnified when the itinerant electrons are confined in two-dimensional (2D) systems^{15–20}. More interestingly, Rashba-type spin-orbit interaction, which relies on the inversion asymmetry could be tuned by simply applying gate voltage^{10,11,21,22}. Thus, the electrical output voltage from the conversion of spin flow, i.e. inverse Edelstein effect (IEE), could be modulated with gate voltage²³. However, this gate effect is transient as it disappears when the gate voltage is turned off. Applying a ferroelectric channel may enable switching of the polarity of inversion asymmetry and allow non-volatile control of spin-charge conversion²⁴. This approach lays out a new concept of memory devices with superior energy efficiency²⁴. Demonstrations of non-volatile spin-charge conversion have recently been achieved in two distinct ferroelectric systems. One is SrTiO₃-based conductive interface²⁴ and the other is ferroelectric GeTe²⁵. However, the ferroelectricity of SrTiO₃ appears only under 40 K²⁴. And ferroelectric property of GeTe is rather weak due to the presence of free carriers²⁵. It is highly challenging to develop relevant systems that retain both ferroelectricity and decent conductivity to function as a tunable spin-charge conversion channel.

In this report, we introduce an alternative control of spin-charge conversion through the non-volatile tuning of Fermi level in graphene. We demonstrate that the sign change of spin-charge conversion can be also achieved by inverting energy-momentum dispersion of Rashba spin texture instead of reversing the polarity of Rashba spin-orbit interaction. Ferroelectric insulator polyvinylidene fluoride-co-trifluoroethylene (PVDF-TrFE) film was employed to tune the Fermi level in between above and below the charge neutral point (CNP) in graphene. The spin accumulation to the inverted electron dispersion with Rashba spin texture leads to opposite shift of momentum. The ferromagnetic resonance (FMR) and IEE results show non-volatile switching of output voltage at room temperature with robust endurance. In addition, tuning Fermi level by using adjacent ferroelectric insulator is electric-field-only process and thus ultralow-power device operation, whereas switching the polarity of ferroelectric conductor involves with large leakage currents. Our approach opens an alternative route for

highly energy-efficient manipulation of spin signal with a promising prospect for the new class of spin-orbitronic devices.

Results

Concept of nonvolatile control of spin-charge conversion in graphene

Figure 1a shows a schematic for non-volatile spin-charge conversion in PVDF-TrFE/graphene/YIG heterostructure. Graphene is a well-known 2D system with outstanding electrical properties and exhibits robust spin-charge conversion when the spin-orbit interaction is implemented through various methods^{26–36}. It has also been shown that the proximity effect from the interfaces with a yttrium iron garnet (Y₃Fe₅O₁₂, YIG) drives Rashba-type spin-orbit interaction as well as spin-charge conversion^{15–18}. Here, ferromagnetic insulator YIG film can also function as a spin source with outstanding low magnetic damping^{37,38}. The propagation of magnon in YIG excited by FMR transfers spin angular moments (J_s , spin current) into graphene. Then, the injected spin current in graphene is altered into a transverse charge current by IEE. Here, the direction of the charge current can be inverted through the poling of the ferroelectric PVDF-TrFE without requiring an additional electric field or magnetic anisotropy. The electrical dipole moment of PVDF-TrFE could tune the Fermi level and thus switch the type of majority carriers between electron and hole in graphene as shown in Fig. 1b.

To examine the impact of the carrier switching in spin-to-charge conversion, we diagonalized the graphene Hamiltonian with Rashba spin-orbit coupling expressed as $H = \hbar v_F (\tau q_x \sigma_x + q_y \sigma_y) + \lambda_{SO} \tau \sigma_z s_z + \lambda_R (\tau \sigma_x s_y - \sigma_y s_x)$, where v_F is the Fermi velocity (without spin-orbit coupling), \mathbf{q} is the relative momentum with respect to the Dirac point, σ and \mathbf{s} are the pseudo-spin and real-spin Pauli matrices, respectively, $\tau = \pm 1$ for K and K' valleys respectively, and λ_{SO} and λ_R are the spin-orbit coupling and the Rashba parameters, respectively^{39,40}. The resulting band structure and the spin texture are illustrated in Fig. 1b. Provided that the spin-orbit coupling and the Rashba parameters are positive, the spin texture is given by $(\mathbf{s}) \parallel \hat{\mathbf{z}} \times \mathbf{q}$ for the higher electron and the lower hole bands and $(\mathbf{s}) \parallel -\hat{\mathbf{z}} \times \mathbf{q}$ for the other. In other words, the spin textures at the Fermi level are equivalent for both above and below the CNP in graphene as long as the polarity of inversion asymmetry induced by the proximity effect from YIG remains unchanged. When the spin angular moment, polarized along the y direction, is accumulated in graphene by spin pumping, the shift of Fermi momentum so does the Fermi contour occurs in the opposite direction between electron doping and hole doping cases (Fig. 1b and c). This leads to net $\pm \Delta k_x$ producing net charge current $\pm J_x$. Thus, the output voltage of IEE changes sign depending on the carrier type of graphene, which can be tuned by the poling of PVDF-TrFE. An explicit demonstration of the carrier dependence of the Edelstein effect is also presented in Supplementary Note 1. In this way, we can control the non-volatile spin-charge conversion in graphene with an electric-field only without reversing inversion asymmetry.

Ferroelectric charging and switching of inverse Edelstein effect

Figure 2a shows an illustration of the studied graphene-based heterostructures for field effect transistor (FET) and FMR-IEE measurement. CVD graphene was transferred on top of epitaxial YIG films. The graphene channel has dimensions of 1 mm width and 5 mm length (see Supplementary Note 2 and Fig. S1 for details). Then, PVDF-TrFE film was spin-coated on graphene. According to XRD results, the spin-coated PVDF-TrFE film is beta phase having a lamellar structure, which leads to out-of-plane ferroelectricity^{41,42} (see Supplementary Note 2 and Fig. S2 for details). MoO₃ film was thermally deposited before the top Au gate electrode to protect the molecular PVDF-TrFE layer and prevent unwanted pinholes.

Figure 2b shows the Field-Effect Transistor (FET) characteristics of the graphene-based heterostructure. The typical characteristic of FET

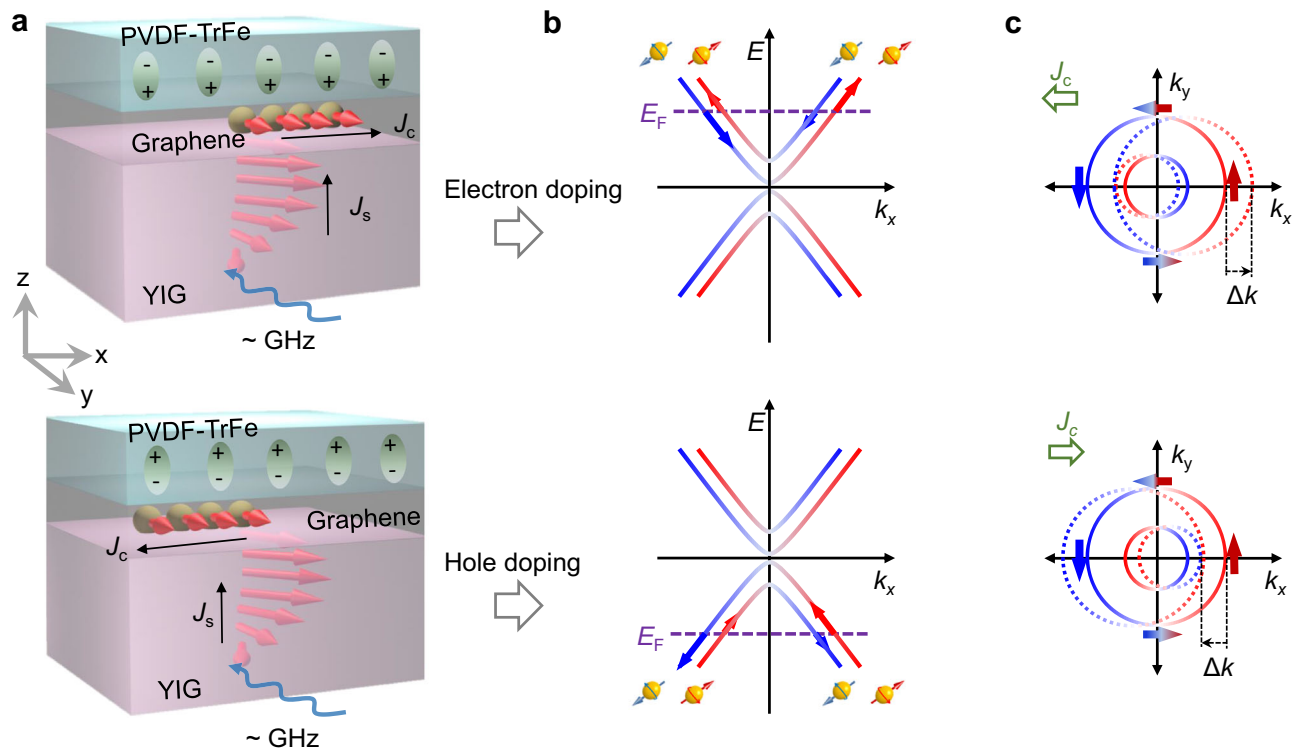


Fig. 1 | Concept for the nonvolatile control of spin-charge conversion via ferroelectric charging. **a** Schematic illustration of the inversion of the spin-charge conversion in single-layer graphene. Vertical spin flow generated by the ferromagnetic resonance is converted into a transverse charge flow via IEE. Here, the direction of charge flow in graphene depends on the poling state of PVDF-TrFE. **b** Spin-split energy dispersion in graphene due to Rashba spin-orbit interaction induced by the proximity effect from YIG. Red and blue lines represent energy dispersion for spin-up and spin-down electrons, respectively. The ferroelectricity of PVDF-TrFE allows the adjustment of the Fermi level in graphene above the CNP

(upper) and below the CNP (lower). Arrows indicate the change of electron distribution when electron spins with polarization of $+y$ is accumulated. **c** Schematic illustration of IEE in graphene when the Fermi level is above the CNP (upper) or below the CNP (lower). When the spins of polarization y are injected into graphene, the shift of the Fermi contour occurs. This Fermi contour shift is toward the opposite direction for each upper and lower case, respectively. Finally, $\pm \Delta k$ in momentum space produces output voltage with a nonvolatile sign change depending on the location of the Fermi level controlled by the poling of ferroelectric PVDF-TrFE.

curve in graphene exhibits a sharp resistance peak at the CNP and rapid decrease of resistance along with doping either electrons or holes by electric field (Supplementary Note 2 and Fig. S3). Due to the ferroelectric poling state of adjacent PVDF-TrFE, FET curves display large shifts depending on the direction of electric field sweeping^{43–45}. As increasing gate bias from -5.19 mV/nm to $+5.19$ mV/nm, the peak of FET curve appears at around $+2.96$ mV/nm, where the ferroelectric polarity reverses. The shift of FET curve occurs to the opposite side as reversing electric field sweeping and it becomes larger with increasing range of electric field sweeping (see Supplementary Fig. S4). Therefore, the positive (negative) electric field pulse, which induces positive (negative) remanent poling state of PVDF-TrFE, makes the graphene to be electron (hole) doping state.

The effect of ferroelectric charging on the spin-charge conversion in graphene can be probed via FMR-IEE experiments. Here, FMR in YIG induces propagation of magnon resulting in spin-pumping at the interface of YIG/graphene. Then, the transferred spin angular momentum in graphene can be converted into the transverse charge current through the IEE. As shown in Fig. 2c, d, the output voltage produced by FMR-IEE displays the non-volatile switching of the spin-charge conversion at room temperature. For a positive electric field pulse ($+5.93$ mV/nm to 0 mV/nm), which induces positive remanence poling state of PVDF-TrFE and electron doping in graphene, the measured V_{IEE} signal exhibits a sharp negative peak at the resonance field. If the graphene is in a hole doping state by negative electric field pulse (-5.93 mV/nm to 0 mV/nm), V_{IEE} exhibits a sharp positive peak. In other words, spin-charge conversion in graphene can be switched in a non-

volatile manner by ferroelectric poling of adjacent PVDF-TrFE as it enables to tune the Fermi level and switch between electron and hole doping. Ab initio density functional theory calculations confirm the shift of CNP via ferroelectric control. As shown in the projected density-of-states plots of PVDF-TrFE/graphene heterostructure (Fig. 2e, f), the CNP of the graphene is shifted by -2 eV through the ferroelectric reversal. Theoretical calculation also shows that the Rashba spin splitting induced by ferroelectric poling is nearly negligible (See Supplementary Fig. S5). Thus, the ferroelectric PVDF-TrFE layer allows to tune the carrier type through the Fermi level shift with negligible impact on the Rashba spin-orbit interaction induced by the YIG film. We note that the underlying YIG film could drive ferromagnetism in graphene through the proximity-induced exchange interaction as previously reported⁴⁶. However, the proximity-induced ferromagnetism in graphene by the adjacent YIG film becomes nearly negligible at room temperature, and thus its impact on the observed FMR-IEE spectra at room temperature can be ignored (See Supplementary Note 3 and Fig. S6).

It is also possible that the inverse spin Hall effect (ISHE) may partially contribute to the observed spin-charge conversion. However, perpendicular injection of spin flow into a 2D system is not likely to generate extrinsic spin Hall effect as it is derived from a series of scattering for the spin-dependent deflection^{47,48}. The intrinsic spin Hall effect would also provide a negligible contribution to spin-charge conversion because the momentum perpendicular to the plane is highly suppressed in 2D systems. The spin-charge conversion in graphene has been more extensively studied in lateral transport

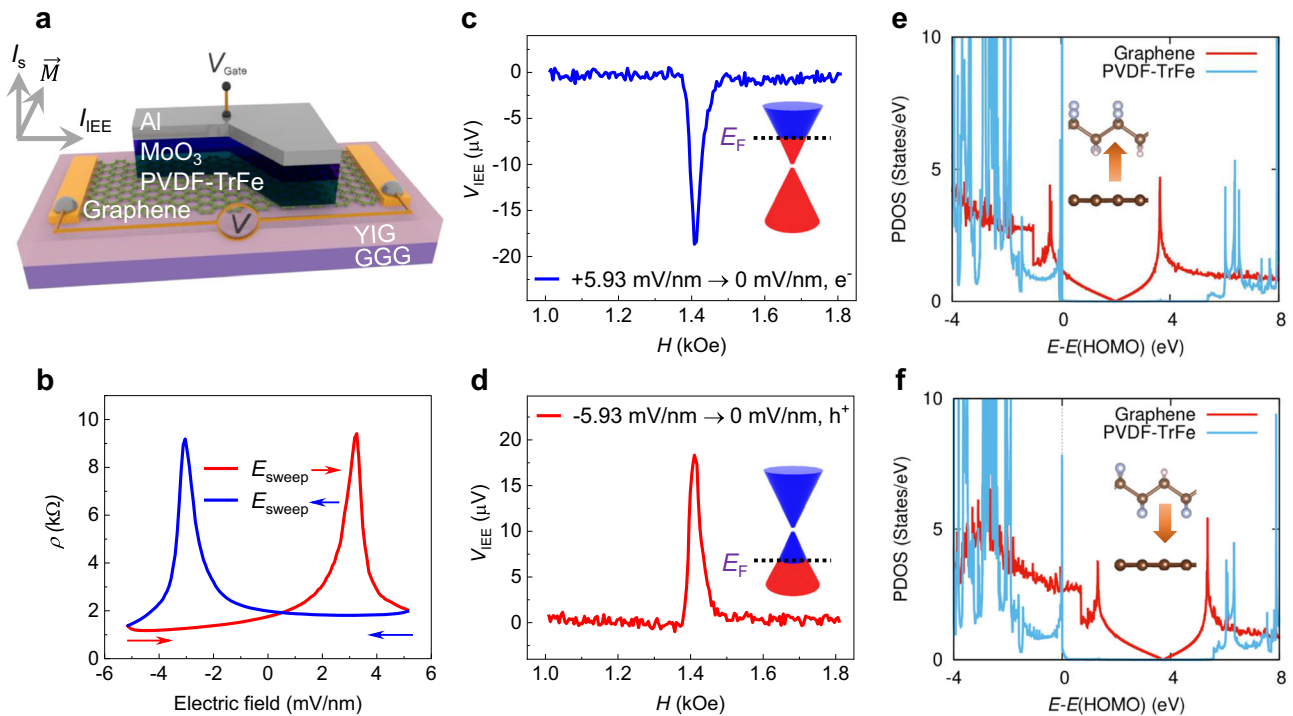


Fig. 2 | FET characteristics and FMR-IEE in graphene-based heterostructure.

a Configuration of the device structure for the study of FET and FMR-IEE characteristics. For FMR-IEE measurements, the sample is placed on top of a coplanar waveguide. **b** Resistivity of graphene as a function of electric field for ± 5.19 mV/nm sweeping ranges at 300 K. The blue line displays FET curve measured by sweeping electric field from +5.93 mV/nm to -5.93 mV/nm, and the red line represents FET curve for opposite electric field sweeping. **c, d** The measured V_{IEE} upon sweeping the in-plane magnetic field at 6 GHz for opposite remanent poling state of PVDF-TrFE. Measurements were performed at room temperature. The positive poling state (**c**) is obtained by increasing electric field up to +5.93 mV/nm and then

removing it to be 0 mV/nm, whereas the negative poling state (**d**) was prepared by the opposite electric field pulse. Each remanent poling state results in a Fermi level above the CNP (electron majority carriers) or below the CNP (hole majority carriers), respectively. The obtained V_{IEE} spectra display sharp peaks with opposite signs for electron and hole doping cases indicating inversion of spin-charge conversion by the ferroelectric charging. **e, f** The PVDF-TrFE/Graphene heterostructures are calculated using the density functional theory method. From the projected density-of-state (PDOS) of graphene depicted by red lines, the CNP is shifted by -2 eV depending on the direction of ferroelectric polarization.

geometry^{30–36}. In such case, symmetry given by the polarization direction of spin flow and its precession in response to the external field allows to distinguish between ISHE and IEE^{31–33}. We note that ISHE observed in lateral transport geometry shows no sign change of output voltage regardless of the location of the Fermi level, instead, it displays rapid decay as the Fermi level moves away from the CNP^{33,49}. Another possible origin for the observed FMR-induced voltage generation is thermoelectric effects. The resonance absorption of microwave could cause local heating and thus voltage across lateral direction due to the Seebeck effect. However, this thermally induced signal should not be associated with the magnetic polarity of YIG. The measured V_{IEE} changes sign with the inversion of the magnetization of YIG, and thus obtained V_{IEE} in our experiments is not associated with thermoelectric effects (See supplementary Note 4 and Fig. S7).

Nonvolatile tuning of spin-charge conversion and its stability

The electric field dependence of spin-charge conversion and its hysteretic behavior due to ferroelectricity are displayed in Fig. 3a and b. The FMR-IEE measurements were performed by first increasing the poling electric field from -5.93 mV/nm to +5.93 mV/nm and then decreasing the poling electric field from +5.93 mV/nm to -5.93 mV/nm. Starting from -5.93 mV/nm, $V_{IEE}(H)$ displays a sharp positive peak and maintains until +3.70 mV/nm and then undergoes inversion when the poling electric field reaches +4.44 mV/nm. In a reverse variation of the poling electric field (+5.93 mV/nm to -5.93 mV/nm), V_{IEE} exhibits complete inversion when the poling electric field reaches -4.44 mV/nm, in consistency with the hysteretic behavior of the adjacent PVDF-TrFE layer. The efficiency of spin-charge conversion, represented by

the inverse Edelstein length (λ_{IEE}), can be estimated once we get the spin mixing conductance at the YIG/graphene interface from the relation, $G_{eff}^{\uparrow\downarrow} = \frac{4\pi M_s t_{FM}}{\hbar\omega} (\Delta H_{YIG/Gr} - \Delta H_{YIG})$ ¹⁸. Where t_{FM} is the FM thickness, \hbar is the reduced Planck constant, ω is the microwave frequency, ΔH_{YIG} is the linewidth of the GGG/YIG, and $\Delta H_{YIG/Gr}$ is the linewidth of the GGG/YIG/graphene/PVDF-TrFE. Finally, λ_{IEE} can be obtained from the relation, $\lambda_{IEE} = \frac{4V_{IEE}^{peak}}{R_s w e f p G_{eff}^{\uparrow\downarrow} (h_{rf}/\Delta H)}$ ¹⁸. Where, R_s is the resistance of the graphene, w is the width of the graphene, p is the precession ellipticity, and h_{rf} is the amplitude of the RF magnetic field. The maximum value obtained for λ_{IEE} is -0.0095 nm at -1.48 mV/nm (see also Supplementary Note 5 and Figs. S8–11), which is similar in magnitude compared to the previously reported λ_{IEE} in graphene-based heterostructures^{16,18}. Figure 3c displays the stability of the remanent poling effect on the spin-charge conversion. The time-dependent FMR-IEE measurements were performed after poling PVDF-TrFE with either a positive (+5.93 mV/nm) or negative (-5.93 mV/nm) electric field pulse. Both of V_{IEE} signals are maintained for over several hours, which demonstrates robust stability of the non-volatile spin-charge conversion within the measurement windows.

The observed non-volatile switching of spin-charge conversion could be attributed to the inversion of Rashba spin-orbit interaction induced by the ferroelectric poling. However, our DFT results showed negligible spin-splitting by the ferroelectric polarization. And the switching of spin-charge conversion in graphene due to the change of the type of majority carriers has been observed in various graphene-based heterostructures^{17,33–35,50}. In order to confirm the origin of spin-

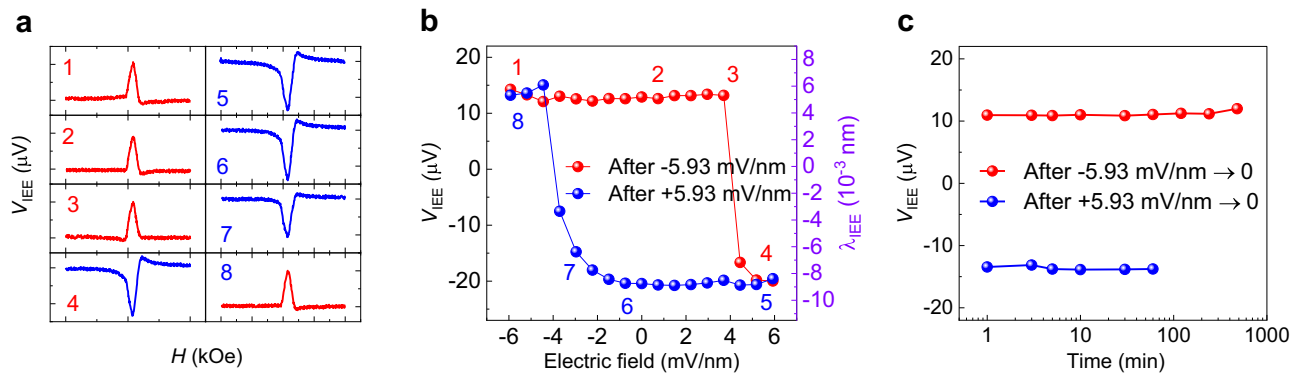


Fig. 3 | Electric field-dependent spin-charge conversion. **a** FMR-IEE voltage (V_{IEE}) as a function of the magnetic field measured at various poling electric fields. Numbers on the top left of each panel represent spectra measured at each electric field poling indicated in **(b)**. All data were recorded with a microwave frequency of 6 GHz. **b** Maximum value of V_{IEE} as a function of poling electric fields. The red symbols are results recorded with increasing poling electric field from -5.93 mV/nm

nm to $+5.93 \text{ mV/nm}$, whereas blue symbols are for decreasing poling electric field from $+5.93 \text{ mV/nm}$ to -5.93 mV/nm . Each measurement was performed after poling the PVDF-TrFE layer. **c** The time-dependent V_{IEE} measured after poling PVDF-TrFE layer with maximum positive or negative electric field pulse ($\pm 5.93 \text{ mV/nm}$). The magnitude of the V_{IEE} signals was maintained over several hundred minutes. Data in **(a, b, and c)** are all recorded at room temperature.

charge conversion in our studied devices, we performed FMR-IEE study with a control device of YIG/graphene (see Supplementary Note 6 and Fig. S12). Instead of ferroelectric PVDF-TrFE, an insulating Parylene layer was used for the top gate. The control device exhibits CNP at around $+1.11 \text{ mV/nm}$. When the electric fields were set to -0.59 mV/nm and $+0.59 \text{ mV/nm}$, reversing the polarity of electric field while maintaining the graphene's carrier type as hole carriers, we observed that the sign of V_{IEE} signal remained unchanged. When the electric fields were set to $+0.59 \text{ mV/nm}$ and $+1.56 \text{ mV/nm}$, maintaining the electric field polarity while changing the carrier type from holes to electrons, we observed a reversal of the V_{IEE} signal. These results reflect that the observed inversion of spin-charge conversion via the ferroelectric poling originated from the change of the Fermi level rather than the change in the polarity of inversion asymmetry.

Discussion

In conclusion, we demonstrated non-volatile control of spin-to-charge current conversion at room temperature, which brings a promising potential to implement new memory and spin logic devices. Instead of manipulating the magnetization direction of ferromagnetic materials as in conventional STT- or SOT-MRAM devices, we focused on controlling the Rashba effect using ferroelectric materials, along with the associated spin-to-charge current conversion. This approach aimed to address the durability issues of soft magnetic-based devices and the thermal stability problems. Additionally, we aimed to realize voltage-based operation, non-volatility, and control over current direction in low-dimensional materials like graphene. Through experimental measurements using FMR at room temperature, we demonstrated that the direction of charge current converted by the graphene carrier type can be controlled by aligning the polarization direction of PVDF-TrFE. This ferroelectric-based control of output signal offers non-volatile characteristics, different from conventional gate-voltage control methods. The complete switching of spin-charge conversion in our system was achieved by applying a electric field pulse over -4.44 mV/nm . Thus, it can evolve into an exceptionally energy-efficient writing process with further development of a relevant thin ferroelectric layer. We note that there have been tremendous efforts to realize non-volatile switching of spin-charge conversion through the inversion of Rashba spin-orbit interaction^{24,25}. However, the ferroelectric channel that allows the inversion of Rashba spin-orbit interaction requires large energy consumption due to strong leakage currents, as evidenced by the electric field required for GeTe²⁵ being two orders of magnitude larger than our system. In contrast, control of spin-charge conversion

through Fermi level tuning with an adjacent insulating ferroelectric layer relies exclusively on electric-field manipulation, making it an outstanding energy-efficient process. Moreover, this non-volatile control of spin-charge conversion by inverting energy-momentum dispersion could be extended to various semiconductors and/or semi-metallic systems other than graphene. Finally, we anticipate that incorporating such ferroelectric-controlled spin-charge conversion can lead to the implementation of new Process-In-Memory (PIM) devices, enabling low-power read/write operations, high integration density, and both memory and computational functionalities.

Methods

Materials preparation

GGG/YIG substrates were cut to dimensions of 8 mm by 8 mm by using the dicing saw and cleaned by using an ultra-sonicator. Then, CVD-graphene with dimensions of 1 mm by 5 mm was transferred on the substrate by using PMMA-based dry transfer method with the thermal release tape^{51,52}. Thermally deposited Au were used for contact electrodes to detect V_{IEE} . The ferroelectric PVDF-TrFE film was coated by using spin coater at 2500 rpm followed by a soft baking process at 110°C for 20 minutes to remove the solvent. Then, a crystallization process was performed in a furnace at 130°C for 6 hours. Molybdenum trioxide (MoO_3) were thermally deposited over the molecular layer of PVDF-TrFE to prevent unwanted pinholes. Finally, aluminum (Al) were deposited by using thermal evaporation for the top gate.

FMR and FMR-IEE measurements

For the FMR measurements, we used the broadband FMR of the PPMS option with a coplanar waveguide (CPW) and a Rohde & Schwarz RF signal generator operated in the frequency range of 2–19 GHz. For the FMR-driven IEE measurements, we used CPW FMR with contact pads for the detection of IEE (RNDWARE Co. Ltd.). Devices used for FMR-IEE studies have a channel size of 1 mm width and 3 mm length with gold contact pads at both sides. Electric field to switch ferroelectric poling was applied using Keithley 2636 A source meter. Voltages generated by FMR-IEE were detected by using Keithley 2182 nanovoltmeter with remanent electric field after applied electric field. All FMR and FMR-IEE measurements were performed in the PPMS chamber at 300 K.

First-principles calculation

We performed the first-principles calculation using the DFT method within the local-density approximation as implemented in VASP^{53,54}. We used an 800 eV plane wave cut-off energy and $10 \times 20 \times 1$ k-points

for all calculations and the projector augmented wave method. During the geometry optimizations, the in-plane lattice constant was fixed at the experimental value of graphene, and the tolerance on atomic forces was set to 0.02 \AA^{-1} . The electronic density of states was calculated using a fine mesh $20 \times 40 \times 1$ k-points.

Data availability

Source data are provided in this paper. Additional data that support the findings of this study are available from the corresponding authors upon reasonable request.

References

- Manipatruni, S. et al. Scalable energy-efficient magnetoelectric spin-orbit logic. *Nature* **565**, 35–42 (2019).
- Slonczewski, J. C. Current-driven excitation of magnetic multilayers. *J. Magn. Mag. Mater.* **159**, L1–L7 (1996).
- Miron, I. M. et al. Perpendicular switching of a single ferromagnetic layer induced by in-plane current injection. *Nature* **476**, 189–193 (2011).
- Apalkov, D., Dieny, B. & Slaughter, J. M. Magnetoresistive random access memory. *Pro. IEEE* **104**, 1796–1830 (2016).
- Dieny, B. et al. Opportunities and challenges for spintronics in the microelectronics industry. *Nat. Electron.* **3**, 446–459 (2020).
- Shao, Q. et al. Roadmap of spin-orbit torques. *IEEE Trans. Mag.* **57**, 1–39 (2021).
- Maruyama, T. et al. Large voltage-induced magnetic anisotropy change in a few atomic layers of iron. *Nat. Nanotechnol.* **4**, 158–161 (2009).
- Bauer, U. et al. Magneto-ionic control of interfacial magnetism. *Nat. Mater.* **14**, 174–181 (2015).
- Vaz, D. C. et al. Voltage-based magnetization switching and reading in magnetoelectric spin-orbit nanodevices. *Nat. Commun.* **15**, 1902 (2024).
- Bychkov, Y. A. & Rashba, E. I. Properties of a 2D electron-gas with lifted spectral degeneracy. *JETP Lett.* **39**, 78–81 (1984).
- Manchon, A., Koo, H. C., Nitta, J., Frolov, S. M. & Duine, R. A. New perspectives for Rashba spin-orbit coupling. *Nat. Mater.* **14**, 871–882 (2015).
- Edelstein, V. M. Spin polarization of conduction electrons induced by electric current in two-dimensional asymmetric electron systems. *Solid State Commun.* **73**, 233–235 (1990).
- Shen, K., Vignale, G. & Raimondi, R. Microscopic theory of the inverse edelstein effect. *Phys. Rev. Lett.* **112**, 096601 (2014).
- Sánchez, J. C. R. et al. Spin-to-charge conversion using Rashba coupling at the interface between non-magnetic materials. *Nat. Commun.* **4**, 2944 (2013).
- Ohshima, R. et al. Observation of spin-charge conversion in chemical-vapor-deposition-grown single-layer graphene. *Appl. Phys. Lett.* **105**, 162410 (2014).
- Mendes, J. B. S. et al. Spin-current to charge-current conversion and magnetoresistance in a hybrid structure of graphene and yttrium iron garnet. *Phys. Rev. Lett.* **115**, 226601 (2015).
- Dushenko, S. et al. Gate-tunable spin-charge conversion and the role of spin-orbit interaction in graphene. *Phys. Rev. Lett.* **116**, 166102 (2016).
- Mendes, J. B. S. et al. Direct detection of induced magnetic moment and efficient spin-to-charge conversion in graphene/ferromagnetic structures. *Phys. Rev. B* **99**, 214446 (2019).
- Park, J. et al. The effect of graphene interlayer at Pt/YIG interface on spin pumping. *J. Alloy. Compd.* **829**, 154534 (2020).
- Bangar, H. et al. Large spin-to-charge conversion at the two-dimensional interface of transition-metal dichalcogenides and permalloy. *ACS Appl. Mater. Interfaces* **14**, 41598–41604 (2022).
- Datta, S. & Das, B. Electronic analog of the electro-optic modulator. *Appl. Phys. Lett.* **56**, 665–667 (1990).
- Koo, H. C. et al. Control of spin precession in a spin-injected field effect transistor. *Science* **325**, 1515–1518 (2009).
- Lesne, E. et al. Highly efficient and tunable spin-to-charge conversion through Rashba coupling at oxide interfaces. *Nat. Mater.* **15**, 1261–1266 (2016).
- Noël, P. et al. Non-volatile electric control of spin-charge conversion in a SrTiO₃ Rashba system. *Nature* **580**, 483–486 (2020).
- Varotto, S. et al. Room-temperature ferroelectric switching of spin-to-charge conversion in germanium telluride. *Nat. Electron.* **4**, 740–747 (2021).
- Chan, K. T., Neaton, J. B. & Cohen, M. L. First-principles study of metal adatom adsorption on graphene. *Phys. Rev. B* **77**, 235430 (2008).
- Marchenko, D. et al. Giant Rashba splitting in graphene due to hybridization with gold. *Nat. Commun.* **3**, 1232 (2012).
- Gmitra, M., Kochan, D. & Fabian, J. Spin-orbit coupling in hydrogenated graphene. *Phys. Rev. Lett.* **110**, 246602 (2013).
- Park, J. et al. Gate-dependent spin hall induced nonlocal resistance and the symmetry of spin-orbit scattering in Au-clustered graphene. *Phys. Rev. B* **95**, 245414 (2017).
- Safeer, C. K. et al. Room-temperature spin hall effect in graphene/MoS₂ van der waals heterostructures. *Nano Lett.* **19**, 1074–1082 (2019).
- Safeer, C. K. et al. Large multidirectional spin-to-charge conversion in low-symmetry semimetal MoTe₂ at room temperature. *Nano Lett.* **19**, 8758–8766 (2019).
- Ghiasi, T. S., Kaverzin, A. A., Blah, P. J. & Van Wees, B. J. Charge-to-spin conversion by the Rashba–Edelstein effect in two-dimensional van der waals heterostructures up to room temperature. *Nano Lett.* **19**, 5959–5966 (2019).
- Benítez, L. A. et al. Tunable room-temperature spin galvanic and spin Hall effects in van der Waals heterostructures. *Nat. Mater.* **19**, 170–175 (2020).
- Li, L. et al. Gate-tunable reversible Rashba–Edelstein effect in a few-layer graphene/2h-tas₂ heterostructure at room temperature. *ACS Nano* **14**, 5251–5259 (2020).
- Hoque, A. M. et al. All-electrical creation and control of spin-galvanic signal in graphene and molybdenum ditelluride heterostructures at room temperature. *Commun. Phys.* **4**, 124 (2021).
- Galceran, R. et al. Control of spin-charge conversion in van der Waals heterostructures. *APL Mater.* **9**, 100901 (2021).
- Serga, A. A., Chumak, A. V. & Hillebrands, B. YIG magnonics. *J. Phys. D: Appl. Phys.* **43**, 264002 (2010).
- Chumak, A. V. et al. Magnon spintronics. *Nat. Phys.* **11**, 453–461 (2015).
- Kane, C. L. & Mele, E. J. Quantum spin hall effect in graphene. *Phys. Rev. Lett.* **95**, 226801 (2005).
- Min, H. et al. Intrinsic and Rashba spin-orbit interactions in graphene sheets. *Phys. Rev. B* **74**, 165310 (2006).
- Lovinger, A. J. Ferroelectric polymers. *Science* **220**, 1115–1121 (1983).
- Naber, R. C. G., Asadi, K., Blom, P. W. M., de Leeuw, D. M. & de Boer, B. Organic Nonvolatile Memory Devices Based on Ferroelectricity. *Adv. Mater.* **22**, 933–945 (2010).
- Zheng, Y. et al. Gate-controlled nonvolatile graphene-ferroelectric memory. *Appl. Phys. Lett.* **94**, 163505 (2009).
- Zheng, Y. et al. Graphene field-effect transistors with ferroelectric gating. *Phys. Rev. Lett.* **105**, 166602 (2010).
- Song, E. B. et al. Robust bi-stable memory operation in single-layer graphene ferroelectric memory. *Appl. Phys. Lett.* **99**, 042109 (2011).
- Wang, Z., Tang, C., Sachs, R., Barlas, Y. & Shi, J. Proximity-induced ferromagnetism in graphene revealed by the anomalous hall effect. *Phys. Rev. Lett.* **114**, 016603 (2015).
- Dyakonov, M. I. & Perel, V. I. Current-induced spin orientation of electrons in semiconductors. *Phys. Lett. A* **35**, 459–460 (1971).

48. Gradhand, M., Fedorov, D. V., Zahn, P. & Mertig, I. Extrinsic spin hall effect from first principles. *Phys. Rev. Lett.* **104**, 186403 (2010).
49. Yang, H. et al. Gate-tunable spin hall effect in an all-light-element heterostructure: graphene with copper oxide. *Nano Lett.* **23**, 4406–4414 (2023).
50. Khokhriakov, D., Hoque, A. M., Karpiak, B. & Dash, S. P. Gate-tunable spin-galvanic effect in graphene-topological insulator van der Waals heterostructures at room temperature. *Nat. Commun.* **11**, 3657 (2020).
51. Li, X. et al. Transfer of large-area graphene films for high-performance transparent conductive electrodes. *Nano Lett.* **9**, 4359–4363 (2009).
52. Suk, J. W. et al. Transfer of CVD-grown monolayer graphene onto arbitrary substrates. *ACS Nano* **5**, 6916–6924 (2011).
53. Kresse, G. & Furthmüller, J. Efficient iterative schemes for ab initio total-energy calculations using a plane-wave basis set. *Phys. Rev. B* **54**, 11169–11186 (1996).
54. Kresse, G. & Joubert, D. From ultrasoft pseudopotentials to the projector augmented-wave method. *Phys. Rev. B* **59**, 1758–1775 (1999).

Acknowledgements

This work was supported by the National Research Foundation of Korea (NRF) grant funded by the Korea government (2020M3F3A2A03082444, 2021R1A2C1008431, and 2021M3H4A1A0305486411). This work was also supported by the Ulsan National Institute of Science and Technology (1.240007.01 and 1.240031.01). J. P. acknowledges the support of the NRF grant funded by the Korea government (2022R1C1C2010737). D.C. acknowledges the support of the NRF grant funded by the Korea government (2022R1A6A3A01087345). B.-C. M. and K.-W. K. acknowledge the KIST institutional program (2E32251). K.-W. K. acknowledges the financial support by the NRF (RS-2024-00334933). C.H.K. was supported by the Institute for Basic Science (IBS-R009-D1). H. J. acknowledges the support of the NRF grant funded by the Korea government (2023R1A2C1007634, RS-2023-00257666). C.W.A. acknowledges support from the Priority Research Centers Program through the NRF funded by the Ministry of Education (2019R1A6A1A11053838).

Author contributions

J.C., J.P., J.-W.Y. conceived the idea and initiated the project. J.C. performed materials preparations, device fabrications, electrical characterizations, FMR-IEE experiments, and data analysis. J. L. and S. L. assisted with materials preparations and device fabrications. S.N., D.C., and J.J. assisted materials characterizations and electrical measurements. C.W.A. prepared the solution of PVDF-TrFE. J.H. and S.-Y.K.

prepared CVD graphene. J.P. assisted materials characterizations and data analysis. H.J. and I. O. assisted FMR-IEE experiments. K.W.K. worked on a theoretical explanation. C.H.K. and H.J. worked on DFT calculation. All the authors participated in the discussion and the preparation of the manuscript.

Competing interests

The authors declare no competing interests.

Additional information

Supplementary information The online version contains supplementary material available at <https://doi.org/10.1038/s41467-024-52835-z>.

Correspondence and requests for materials should be addressed to Jungmin Park, Choong H. Kim, Kyoung-Whan Kim or Jung-Woo Yoo.

Peer review information *Nature Communications* thanks Saroj Dash, and the other, anonymous, reviewer(s) for their contribution to the peer review of this work. A peer review file is available.

Reprints and permissions information is available at <http://www.nature.com/reprints>

Publisher's note Springer Nature remains neutral with regard to jurisdictional claims in published maps and institutional affiliations.

Open Access This article is licensed under a Creative Commons Attribution-NonCommercial-NoDerivatives 4.0 International License, which permits any non-commercial use, sharing, distribution and reproduction in any medium or format, as long as you give appropriate credit to the original author(s) and the source, provide a link to the Creative Commons licence, and indicate if you modified the licensed material. You do not have permission under this licence to share adapted material derived from this article or parts of it. The images or other third party material in this article are included in the article's Creative Commons licence, unless indicated otherwise in a credit line to the material. If material is not included in the article's Creative Commons licence and your intended use is not permitted by statutory regulation or exceeds the permitted use, you will need to obtain permission directly from the copyright holder. To view a copy of this licence, visit <http://creativecommons.org/licenses/by-nc-nd/4.0/>.

© The Author(s) 2024